Estuary-on-a-chip Unexpected results for the fate and transport of nanoparticles

Julien Gigault, Marianne Balaresque, Hervé Tabuteau

Estuary-on-a-chip: unexpected results for nanoparticles fate and transport

Julien Gigault[1]*, Marianne Balaresque[1], Hervé Tabuteau*[2],

[1]Laboratoire Géosciences Rennes,
UMR6118 CNRS/Université de Rennes1,
263 Av. Général Leclerc, 35000 Rennes
*julien.gigault@univ-rennes1.fr

[2]Institut de Physique de Rennes,
UMR6251 CNRS/Université Rennes 1,
263 Av. Général Leclerc, 35000 Rennes
*herve.tabuteau@univ-rennes1.fr

Abstract

The aim of this work is to evaluate the influence of a spatial salinity gradient, as encountered in an estuarine when fresh water meets salty one, on the aggregation features of fullerene nanoparticles aggregates (nC_{60}). To model these environmental conditions, we design a specific microfluidic device. In literature, physical phenomena occurring in estuarine area, such as the salinity gradient and the flow conditions, were never considered. Our results suggest that even a short time exposure (couple of seconds) to a salinity gradient, i.e. dynamical spatial conditions, profoundly affects the aggregation properties of nanoparticles and therefore their environmental behavior and fate. It appears that a salinity gradient could enhanced the stability of nanoparticles, especially at high ionic strength (closed to the seawater level one). Contrary to the common approach of particle aggregation in the lab in environmental conditions, our study shows the need to reconsider the spatial and temporal variation of abiotic parameters (ionic strength, pH, organic matter concentration) in the understanding and the evaluation of nanoparticles environmental fate and transportation mechanisms.

Keywords: nanoparticles, fate, estuary, aggregation**,** microfluidic, lab-on-a-chip

Introduction

Because the main route of contaminant transport is river, estuarine systems are one of the most targeted environmental compartment. Those ones are known to play a decisive role in the conditioning of the colloidal materials life cycle[1,2]. Estuarine systems are characterized by specific physical and chemical conditions: salinity gradient, wastewater income, organic matter, and human pressure (industrial and agricultural activities). From all these parameters the ionic strength, characterized by the salinity, and the organic matter are the main parameters that affect the stability of micro-nanoscale materials [1,3].

Over the last ten years, the influence of the ionic strength (IS) on the physical and chemical properties of nanoparticles is one of the most studied parameter, for both carbon-based (fullerene, carbon nanotubes)[4–9] and metal-based (Ag, Au, TiO_2) nanomaterials[10–14]. To do so, the kinetic of nanoparticles aggregation is generally determined by monitoring their size evolution according to the time after an addition of a known concentration of electrolyte in the bulk. However, since this measurement is made while the bulk salt concentration is supposed to be homogeneous, it cannot be representative to what happens in the natural environment. Indeed, these experiments are performed in static or large scale dynamic reactors (such as columns) that are not representative of the natural conditions in which there are spatial and temporal variations of the salt concentration. Indeed, the major issue in the environmental media studies (in bulk liquid and porous media) is the limited applicability to the real dynamic process affecting the transport of particles at environmental scale. More generally NPs behaviors in the environment results from various physical and chemical heterogeneities that the NPs come across. For estuarine system, the salinity gradient is one of these spatial and temporal heterogeneities, and up to now nobody has considered its influence on the fate of NPs.

1   Recently, new experimental methods and capacities, based on microfluidic devices, are

2   opening the door to environmental science for better understand the fate of species in dynamic

3   systems, closer to real natural conditions [15–18]. The aim of this work is to evaluate the fate of

4   nanoparticles, using fullerene aggregates (nC_{60}), in a salinity gradient. To do that we

5   developed a specific microfluidic device to simulate an environmentally representative

6   salinity gradient. Our results, compared to classical batch experiments, demonstrates a

7   different and specific aggregation kinetics, which raise new questions and concerns of the

8   existing knowledge on the environmental fate of nanoparticles in estuarine system.

9
10   **Experimental**
11

12   *Sample preparation*

13   nC_{60} were prepared according to classical procedure previously described [19–21]. Typically, 80

14   mg of C_{60} powder (VWR, Fontenay-sous-Bois) were placed in an Erlenmeyer flask with 200

15   mL of deionized (DI) water (18.2 MΩ.cm at 25°C) and continuously stirred for 2 weeks.

16   Finally, the final fullerene aggregates solution (nC_{60}) was filtered at 0.45 μm to remove large

17   aggregates. The final concentration of nC_{60} is 7.2±0.7 μg g^{-1} and was characterized by both

18   Total Organic Carbon analyzer (Shimadzu, TOC-Vcph) and UV-Vis (Perkin Elmer

19   spectrophotometer, Lambda 650). The corresponding size distribution of the nC_{60} initial stock

20   solution is d_{zH}=180.7 nm (with a polydispersity index, PDI=0.07) and is determined by in-situ

21   dynamic light scattering (Vasco-Flex, Cordouan Technologies, France). Preparation of nC_{60}

22   solutions were replicated 8 times with similar size distribution (see Electronic Supplemental

23   Information, Fig. S1).

24

25   *Microfluidic reactor design and operation*

1 We design a microfluidic device to simulate the estuarine salinity gradient (figure 1). We used

2 standard soft lithography to make this microfluidic channel[22]. First we used a negative

3 photoresist resin (Su8 2050 Microchem) that was spin coated on a silicon wafer, heated and

4 cured with UV light through a mask on which the outline of the channel is printed. The resin

5 is again heated and developed in a bath of PGMEA to remove the uncured part of the resin.

6 Thereafter we cast polydimethylsiloxane (PDMS, Sylgard 184 silicone elastomer kit, Dow

7 Corning) on the SU8 master. Once cured at 70°C for an hour the PDMS slab becomes solid, it

8 is removed from the mold and punched to get the inlets and outlets holes of our channel. Then

9 the channel is sealed by gluing the slab on a glass plate using a plasma cleaner (Harrick

10 Plasma). This process renders the surface of the PDMS channel hydrophilic. To recover a

11 hydrophobic surface we put the microfluidic device in an oven at 120°C for two hours. We

12 inject fluid in the channel thanks to syringe pumps (KDS) at the inlets. In a typical

13 experiment, we first saturate the channel with pure water and then connect pure water or salty

14 on one inlet and a dilute fullerenes suspension on the other. The flow rates were controlled by

15 syringe pump from 0.1 to 1.0 ml/h. At those rates the channel is filled in less than a couple of

16 seconds.

17 The microfluidic device is composed of 5 mm long and 200 µm wide inlets and outlets ("A

18 out" and "B out") arms on either side of a 3cm long channel with a width of 800 µm and a

19 height of 75 µm (figure 1). In the following we focus on a given flow rate equals to 1.0 ml/h

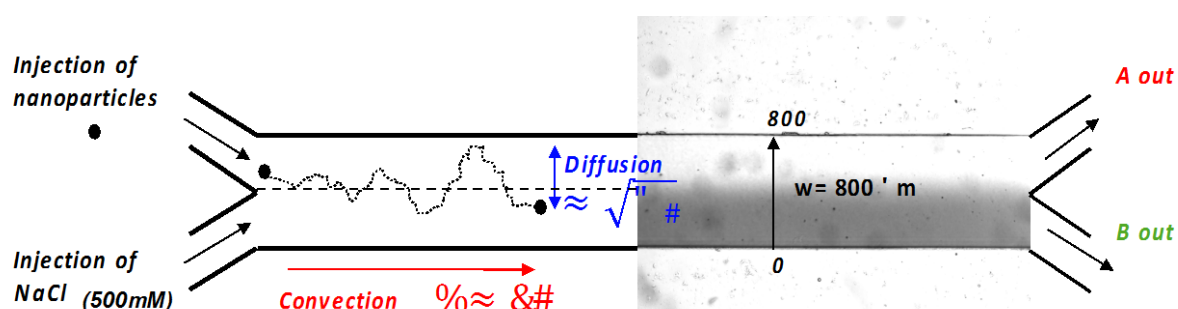20 but we get similar results over a wide range of flow rates (0.1 to 1.0 ml/h).

21

The Figure 1 illustrate the microfluidic device used to simulate the estuarine salinity gradient. Each microfluidic experiment are performed in three steps:

1-*Salt calibration*. We first inject pure water and a salty blue dye solution (Patent Blue from Sigma Aldrich, #198218). This configuration allows us to visualize the salinity gradient on the image that can be analyzed (Fig. S2 top). We checked that the dye does not affect the salinity gradient. The average salt concentration at the two outlets were determined thanks to the UV-spectra of the NaCl stock solution for various salt concentration (Fig. S2 middle and bottom). To this end we collect samples at both outlets during one hour and then we determine absorbance spectrum of the salty solutions.

2-*Diffusion nC_{60} in the MD*. We inject, at a flow rate of 1 ml/h, nC_{60} dispersed in water in one arm and pure water in the other. We collect samples at the two outlets during one hour, we stop the flow and then we determine the size distribution of the NPs. We found the same distribution for both outlets (Fig. S3). This check step confirms that nC_{60} diffuse around as it flows through the microchip, i.e, the particle concentration is symmetric with respect to the middle vertical plane of the straight channel.

3- *nC_{60} aggregates in the salinity gradient*. We inject at a flow rate of 1 ml/h in each inlet arm respectively dilute suspension of nC_{60} in DI water and a salty dye solution (patent blue dissolved in 500 mM of NaCl), a salinity that is encountered in the vicinity of Estuary mouths (~30 g L^{-1}). In this experiment the average NaCl concentration is 42 mmol L^{-1} and 427 mmol L^{-1} for A and B outlets, respectively. The residence time of the nC_{60} in the salinity gradient is lower than 3s in average. Again, after one hour of sample collection at the two outlets the flow rate was stopped and we start measuring the temporal evolution of the nC_{60} size distribution at the two outlets for two hours. Thereafter we compare the temporal evolution of the size distribution of the nC_{60} aggregates with that of a batch experiment as described in

1   literature, i.e. dropwise concentrated NaCl dispersed into a nC_{60} solution and then manually

2   stirred. All the experiments were replicated five times using for each replicate a new nC_{60}

3   stock solution and NaCl preparation.

4

5   *Size characterization by Dynamic Light Scattering*

6   We performed dynamic light scattering measurements within the collection vials connected to

7   both outlets in order to both monitor and determine in real time the presence and the size

8   distribution of fullerene nanoparticles aggregates transported through the microchip.

9   Thanks to an optical fiber remote head, the system used in this work is a dedicated DLS

10 system for contact less in-situ measurement (see ESI, Fig S4). For the nanoparticles setup,

11 DLS specifications were: laser of 658 nm with a 60mW power; the scattering angle is 170°,

12 the working distance is fixed at 80 mm.

13 For nC_{60} size kinetics determination with the NaCl, the intensity-weighted mean diameter (i.e.

14 called the z-average hydrodynamic diameter, d_{zH}) variation was used and was derived using

15 the *Cumulants* algorithm from the auto-correlation function (ACF)[23,24]. *Cumulants* is the

16 simplest analysis of the ACF and is ideal to determine the average particle size of a

17 population. For obtaining size distribution from the autocorrelation curve (ACF function), two

18 algorithms were used: Sparse-Batesian-Learning (SBL) and the Cumulants. Cumulants

19 algorithm is one of the most famous and recognized method for determining size distribution

20 of polydisperse sample (Kopel). In the case of environmental and/or highly polydisperse

21 sample, Cumulants method presents several disadvantages. Indeed, this algorithm doesn't

22 permit independent determination of the long-time baseline of the ACF function and can lead

23 to inconsistent results when different numbers of data points are included in the fit. Using the

24 baseline as a floating parameter makes it possible to detect problems in the data and to fit data

25 when a little bit of noise is present, which our case. The d_H size distribution was determined

26 using the *Sparse Bayesian learning* (SBL) algorithm for the Laplace transform inversion[25].

1   This algorithm is adapted to identify, discriminate and determine the presence of several

2   polydisperse population from the ACF coming from the scattered light[25]. More specifically, it

3   generates a set of sparse solutions of several domains but of the same dimension. Then, it

4   superimposes these solutions to give a global solution with its dimension treated as a

5   regularization parameter. An optimal solution providing a reliable description of a colloidal

6   suspension is determined by an L-curve for selecting the suitable value of the regularization

7   parameter. So, the final result corresponds to the most probable physical solution of the

8   algorithm which position is easily defined as the inflexion of a L-curve representation. This

9   method was proved to be more robust than classical methods used to determine size

10 distribution of polydisperse sample.

11

12 **Results and Discussion**

13 Here our objective is to show that the aggregate growth of nanoparticles depends strongly on

14 the homogeneity of the salt concentration. To do this we compare on Figure 2 the temporal

15 variation of the average hydrodynamic diameter, d_{zH}, of nC_{60} aggregates either obtained by

16 dropwise NaCl into the bulk, at two concentrations 85 and 500 mmol L^{-1}, (named bulk

17 experiments, BE), or collected at the outlets of our microfluidic device (named MD), A_{out} and

18 B_{out}, with an average salt concentration of 42 and 427 mmol L^{-1}, respectively. Both salt

19 concentration in the BE have been chosen to be very close to those obtained at the two outlets

20 of the MD. We choose the two salt concentrations in order to be on both sides of the critical

21 coagulation concentration (CCC) of nC_{60}, which is between 120 and 260 mM of sodium

22 chloride[4–6,26] according to the different formation pathways[21].

23 BE is generally performed to mimic the evolution of the aggregation features of nanoparticles

24 in salty natural environments, i.e., in the ocean or in Estuaries. In this case, the aggregation of

25 nC_{60} takes place in a spatially homogeneous salt concentration. Indeed the salt dispersed at

the beginning of the experiment diffuse so quickly throughout the vial that no significant

aggregates growth of nC_{60} is observed during this homogenization process. In the MD

experiment the fullerene aggregates (nC_{60}) quickly passed through a NaCl gradient and then

they can grow into a vial at rest, in the same conditions than those of the BE.

- Below the CCC of (nC_{60}) there is a slight increase of the aggregates sizes at the beginning of

the experiment (t< 15 min) for the BE and then there is no temporal evolution of d_{zH} anymore

(Fig. 2a, blue circle). The screening of the surface charge is limited at electrolyte

concentrations below the CCC and thus nC_{60} aggregation is limited. In this electrolyte

conditions, the nC_{60} suspension remains quite stable.

We found similar results for the microfluidic experiment in the outlet A_{out} (Fig. 2a, black

circle). This is further confirmed by looking at the global size distribution summed over the

total kinetics time for both types of experiment (Fig. 2b), which are very similar. The mean

aggregate size is a bit larger in the BE than in the MD experiment since the salt concentration

is slightly higher in the former case. However, it is worth noting that there is a small micron

size population (d_{zH}>1μm) in the MD experiment, which is not the case in the BE. We will

get back to this point later on.

-Above CCC of (nC_{60}) the situation is completely different whether the nC_{60} aggregates

encounter a spatial salt gradient or not (Fig. 2c). In the BE d_{zH} increases over time, up to 400

nm. A similar trend was previously observed in literature, which validates our bulk

experiments strategy [26]. As expected, above the CCC, the nanoparticle surface charge is

completely screened, thus eliminating the energy barrier to aggregation. Surprisingly, for

roughly the same amount of salt at the outlet B of the microchip there is only a limited

aggregate growth while we are well above the CCC, d_{zH} increasing slightly from 170 nm and

levels of around 260 nm. We do not observe any further growth after two hours. Two distinct

aggregate size distributions (Fig. 2d) were obtained for Bout and 500mM for the BE. For the

BE, the first population at 170 nm corresponds to the initial population of nC_{60}, while the second population at 450 nm corresponds to the nC_{60} aggregates induced by NaCl. This means that one part of the nC_{60} aggregates that belongs to this initial population has not yet partake to the aggregation process. If the experiment would have last longer this first population would have disappeared progressively. In the MD experiment we also have two aggregate populations. However in the MD experiment, contrary to BE, the initial population is predominant in the size distribution. There is only a slight shift of the average aggregate size, from 170 to 250 nm. Therefore in this case the aggregation mechanism is quite different than before, for the BE. Moreover, as for A_{out}, a micro-sized population is still observed but with much larger contribution to the overall population of B_{out}. We suppose that there is a release of micron-sized aggregates of nC_{60} formed in the MD. Nevertheless, their quantity is relatively low compare to the nano-sized population (170 nm) due to the dependence of intensity of light scattered (I) with size (r^6) and concentration c.
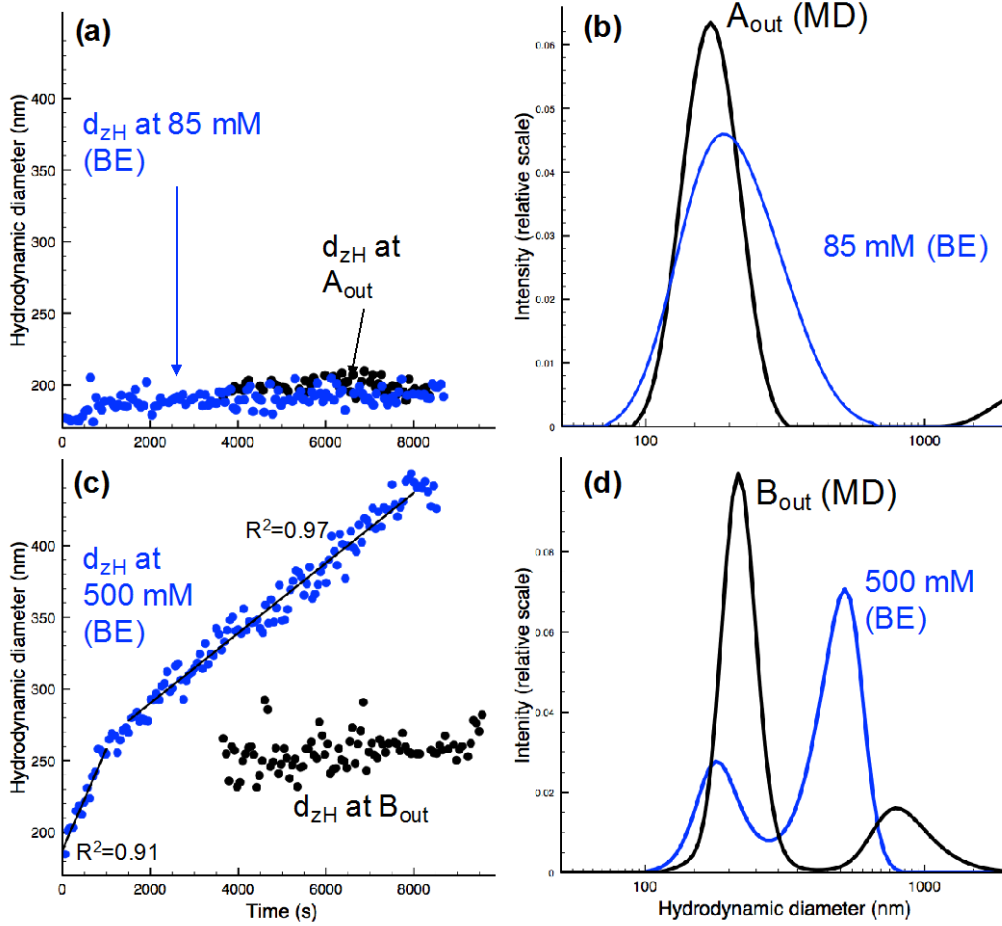
Figure 2: (a,c) illustration of the z-average hydrodynamic diameter (nm), determined by the Cumulants algorithm, according to the ionic strength using bulk experiment and the use of MD (A_{out} and B_{out}) (b,d) the average hydrodynamic diameter distribution determined by SBL algorithm and integrated along the whole duration of the kinetics (8500 and 4500 s for bulk an MD experiments, respectively). On (c) for 500 mM (BE), there are two linear fits of the data ($d_{zH} = a.T$, with $a=0.064$ and $a=0.023$ for larger values).

8   Several hypotheses can be made to explain the difference between the particle aggregation in

9   the bulk and the microfluidic experiment.

10   o   First, the difference between microfluidics and the bulk experiments could be

11   explained by the Diffusion-Limited Colloidal Aggregation (DLCA) and Reaction-

12   Limited Colloidal Aggregation (RLCA) mechanisms[27]. Indeed, it is well known that in

13   batch mode, DLCA is the predominant behavior, where no repulsive barrier exists

14   between the particles and the aggregate growth rate is entirely driven by Brownian

15   motion. DLCA induces the formation of open structure aggregates, with fractal

16   dimension (D_f) generally ranging between 1.5 and 2.0 with a linear increase of the

| 1 | aggregate size over time [5,26], as we also obtained here (Fig. 2.c). In the other case, |
2	where there is a repulsive energy barrier between fullerene particles, RLCA is
3	dominant with a limited aggregate growth, contrary to DLCA, as it was observed in
4	case of the microfluidic experiment presented in this work. This result suggests that
5	the salt gradient causes the nC_{60} aggregation according to the RLCA mode and
6	thereafter remains stable in time over our experimental window.
7	o Secondly, during the transportation of nC_{60} through the microchip, after several hours
8	of experiments and replicates larger aggregates can be formed in the salt front
9	localized at the center of the channel corresponding to the black line in fig. 3.
10	Indeed, this black-like deposition is characteristic of fullerene aggregates and is
11	localized at the middle of the salt gradient. If too large aggregates could be formed,
12	the micron-sized fraction of those sediment into the MD (Fig. 3). This hypothesis
13	would confirm that micron-sized particles released in A_{out} and B_{out} are aggregates
14	formed mainly within the salinity gradient in the MD. Nevertheless, this hypothesis
15	cannot explain why the other part of the size distribution, small particles still present
16	in B_{out} at high [NaCl] (i.e. >CCC), do not form greater aggregates over time, as big as
17	those observed in bulk experiments.

d nC_{60} aggregates

18
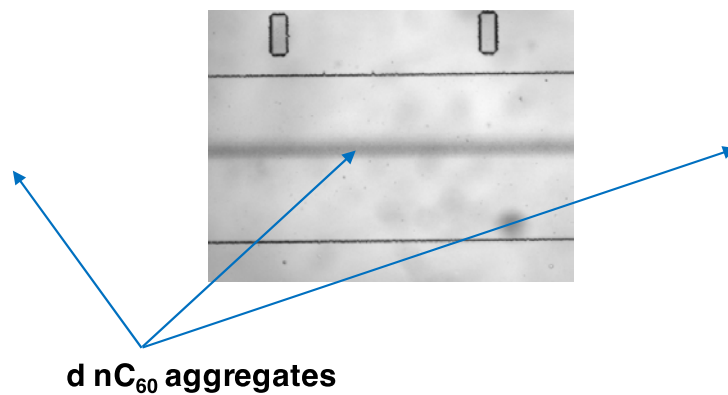
19 *Figure 3: Illustration of the MD with deposition of nC_{60} micron-sized aggregates in the center of the channel (dark lines)*
20 *after several cycles of operation and replicates*

Due to the NaCl concentrations used in this study, no representative electronic microscopy image of the nC_{60} aggregates can be obtained. But, despite the different hypotheses described above, it appears clearly that nC_{60} are transported and diffused through the salinity gradient. During this short time transportation within the salinity gradient, a clear difference on the aggregation behavior is identified, compared to the classical results in bulk experiments.

Environmental implication

Based on these results and comparing to the literature concerning the environmental behavior of manufactured nanomaterials, several questions raised up. Indeed, both incidental and manufactured nanoparticles are expected to be released massively closed to urban system that will be eventually released in the river and finally transport through the estuarine system characterized by an increasing ionic strength. The expectations are that nanoparticles (NPs) will settle at different rate when the ionic strength increases. In literature, physical phenomena occurring in estuarine area, such as the salinity gradient and various flow conditions, were never considered. But, our results suggest that a short exposition of NP such as nC_{60} within the salinity gradient affects definitely their aggregation mechanisms, and therefore their environmental behavior. Secondly, the scientific community on colloids and nanoparticles agrees to the fact that an ionic strength closed to the seawater ones leads to an irreversible aggregation and a change in size (up to micrometer). Our results suggest that the salinity gradient could enhanced the stability of nanoparticles, especially at high ionic strength (closed to the seawater one). This first study shows the need to reconsider the spatial and temporal variation of abiotic parameters (ionic strength, pH, organic matter concentration) in the

understanding and the evaluation of nanoparticles environmental fate and transportation mechanisms.

Reference

(1)   Mayer, L. M.; Wells, M. L. Aggregation of Colloids in Estuaries. In *Treatise on Estuarine and Coastal Science*; 2012; Vol. 4, pp 143–160.

(2)   Lasareva, E. V.; Parfenova, A. M.; Demina, T. S.; Romanova, N. D.; Belyaev, N. A.; Romankevich, E. A. Transport of the Colloid Matter of Riverine Runoff through Estuaries. *Oceanology* **2017**, *57* (4), 520–529.

(3)   Hotze, E. M.; Phenrat, T.; Lowry, G. V. Nanoparticle Aggregation: Challenges to Understanding Transport and Reactivity in the Environment. *J. Environ. Qual.* **2010**, *39* (6), 1909–1924.

(4)   Yang, Y.; Nakada, N.; Nakajima, R.; Yasojima, M.; Wang, C.; Tanaka, H. PH, Ionic Strength and Dissolved Organic Matter Alter Aggregation of Fullerene C60 Nanoparticles Suspensions in Wastewater. *J. Hazard. Mater.* **2013**, *244–245*, 582–587.

(5)   Chen, K. L.; Elimelech, M. Aggregation and Deposition Kinetics of Fullerene (C60) Nanoparticles. *Langmuir* **2006**, *22* (26), 10994–11001.

(6)   Chen, K. L.; Elimelech, M. Influence of Humic Acid on the Aggregation Kinetics of Fullerene (C60) Nanoparticles in Monovalent and Divalent Electrolyte Solutions. *J. Colloid Interface Sci.* **2007**, *309* (1), 126–134.

(7)   Brant, J.; Lecoanet, H.; Wiesner, M. R. Aggregation and Deposition Characteristics of Fullerene Nanoparticles in Aqueous Systems. *J. Nanoparticle Res.* **2005**, *7* (4–5), 545–553.

(8)   Chen, Q.; Saltiel, C.; Manickavasagam, S.; Schadler, L. S.; Siegel, R. W.; Yang, H. Aggregation Behavior of Single-Walled Carbon Nanotubes in Dilute Aqueous Suspension. *J. Colloid Interface Sci. //*, *280* (1), 91–97.

(9)   Gigault, J.; Grassl, B.; Lespes, G. Size Characterization of the Associations between Carbon Nanotubes and Humic Acids in Aqueous Media by Asymmetrical Flow Field-Flow Fractionation Combined with Multi-Angle Light Scattering. *Chemosphere* **2012**, *86* (2), 177–182.

(10)   Badawy, A. M. E.; Luxton, T. P.; Silva, R. G.; Scheckel, K. G.; Suidan, M. T.; Tolaymat, T. M. Impact of Environmental Conditions (PH, Ionic Strength, and Electrolyte Type) on the Surface Charge and Aggregation of Silver Nanoparticles Suspensions. *Environ. Sci. Technol.* **2010**, *44* (4), 1260–1266.

(11)   Domingos, R. F.; Tufenkji, N.; Wilkinson, K. J. Aggregation of Titanium Dioxide Nanoparticles: Role of a Fulvic Acid. *Environ. Sci. Technol. //*, *43* (5), 1282–1286.

(12)   Delay, M.; Dolt, T.; Woellhaf, A.; Sembritzki, R.; Frimmel, F. H. Interactions and

Stability of Silver Nanoparticles in the Aqueous Phase: Influence of Natural Organic Matter (NOM) and Ionic Strength. *J. Chromatogr. A //*, *1218* (27), 4206–4212.

(13)   Rahman, T.; George, J.; Shipley, H. J. Transport of Aluminum Oxide Nanoparticles in Saturated Sand: Effects of Ionic Strength, Flow Rate, and Nanoparticle Concentration. *Sci. Total Environ.* **2013**, *463*, 565–571.

(14)   Merschel, G.; Bau, M.; Dantas, E. L. Contrasting Impact of Organic and Inorganic Nanoparticles and Colloids on the Behavior of Particle-Reactive Elements in Tropical Estuaries: An Experimental Study. *Geochim. Cosmochim. Acta* **2017**, *197*, 1–13.

(15)   Sun, C.; Chen, S.-T.; Hsiao, P.-J. Mapping the Salinity Gradient in a Microfluidic Device with Schlieren Imaging. *Sensors* **2015**, *15* (5), 11587–11600.

(16)   Drescher, K.; Shen, Y.; Bassler, B. L.; Stone, H. A. Biofilm Streamers Cause Catastrophic Disruption of Flow with Consequences for Environmental and Medical Systems. *Proc. Natl. Acad. Sci.* **2013**, *110* (11), 4345–4350.

(17)   Dunphy Guzman, K. A.; Finnegan, M. P.; Banfield, J. F. Influence of Surface Potential on Aggregation and Transport of Titania Nanoparticles. *Environ. Sci. Technol.* **2006**, *40* (24), 7688–7693.

(18)   Stocker, R.; Seymour, J. R.; Samadani, A.; Hunt, D. E.; Polz, M. F. Rapid Chemotactic Response Enables Marine Bacteria to Exploit Ephemeral Microscale Nutrient Patches. *Proc. Natl. Acad. Sci.* **2008**, *105* (11), 4209–4214.

(19)   Brant, J. A.; Labille, J.; Bottero, J.-Y.; Wiesner, M. R. Characterizing the Impact of Preparation Method on Fullerene Cluster Structure and Chemistry. *Langmuir* **2006**, *22* (8), 3878–3885.

(20)   Labille, J.; Masion, A.; Ziarelli, F.; Rose, J.; Brant, J.; Villiéras, F.; Pelletier, M.; Borschneck, D.; Wiesner, M. R.; Bottero, J. Y. Hydration and Dispersion of C60 in Aqueous Systems: The Nature of Water-Fullerene Interactions. *Langmuir* **2009**, *25* (19), 11232–11235.

(21)   Gigault, J.; Budzinski, H. Selection of an Appropriate Aqueous Nano-Fullerene (NC60) Preparation Protocol for Studying Its Environmental Fate and Behavior. *TrAC - Trends Anal. Chem.* **2016**, *80*, 1–11.

(22)   Duffy, D. C.; McDonald, J. C.; Schueller, O. J. A.; Whitesides, G. M. Rapid Prototyping of Microfluidic Systems in Poly(Dimethylsiloxane). *Anal. Chem.* **1998**, *70* (23), 4974–4984.

(23)   Koppel, D. E. Analysis of Macromolecular Polydispersity in Intensity Correlation Spectroscopy: The Method of Cumulants. *J. Chem. Phys.* **1972**, *57* (11), 4814–4820.

(24)   Ross Hallett, F. Particle Size Analysis by Dynamic Light Scattering. *Food Res. Int.* **1994**, *27* (2), 195–198.

(25)   Nyeo, S.-L.; Ansari, R. R. Sparse Bayesian Learning for the Laplace Transform Inversion in Dynamic Light Scattering. *J. Comput. Appl. Math.* **2011**, *235* (8), 2861–2872.

(26)   Meng, Z.; Hashmi, S. M.; Elimelech, M. Aggregation Rate and Fractal Dimension of Fullerene Nanoparticles via Simultaneous Multiangle Static and Dynamic Light Scattering Measurement. *J. Colloid Interface Sci.* **2013**, *392*, 27–33.

(27)   Tang, S.; Preece, J. M.; McFarlane, C. M.; Zhang, Z. Fractal Morphology and Breakage of DLCA and RLCA Aggregates. *J. Colloid Interface Sci.* **2000**, *221* (1), 114–123.